THE JOURNAL OF BIOLOGICAL CHEMISTRY VOL. 286, NO. 15, pp. 13681–13694, April 15, 2011

Rif-mDia1 Interaction Is Involved in Filopodium Formation Independent of Cdc42 and Rac Effectors[S]

Received for publication, September 8, 2010, and in revised form, February 16, 2011 Published, JBC Papers in Press, February 21, 2011, DOI 10.1074/jbc.M110.182683

Wah Ing Goh, Thankiah Sudhaharan, Kim Buay Lim[1], Kai Ping Sem, Chew Ling Lau[2], and Sohail Ahmed[3]

From the Institute of Medical Biology, 8A Biomedical Grove, Immunos, Singapore 138648

Filopodia are cellular protrusions important for axon guidance, embryonic development, and wound healing. The Rho GTPase Cdc42 is the best studied inducer of filopodium formation, and several of its effectors and their interacting partners have been linked to the process. These include IRSp53, N-WASP, Mena, and Eps8. The Rho GTPase, Rif, also drives filopodium formation. The signaling pathway by which Rif induces filopodia is poorly understood, with mDia2 being the only protein implicated to date. It is thus not clear how distinct the Rif-driven pathway for filopodium formation is from the one mediated by Cdc42. In this study, we characterize the dynamics of Rif-induced filopodia by time lapse imaging of live neuronal cells and show that Rif drives filopodium formation via an independent pathway that does not involve the Cdc42 effectors N-WASP and IRSp53, the IRSp53 binding partner Mena, or the Rac effectors WAVE1 and WAVE2. Rif formed filopodia in the absence of N-WASP or Mena and when IRSp53, WAVE1, or WAVE2 was knocked down by RNAi. Rif-mediated filopodial protrusion was instead reduced by silencing mDia1 expression or overexpressing a dominant negative mutant of mDia1. mDia1 on its own was able to form filopodia. Data from acceptor photobleaching FRET studies of protein-protein interaction demonstrate that Rif interacts directly with mDia1 in filopodia but not with mDia2. Taken together, these results suggest a novel pathway for filopodia formation via Rif and mDia1.

Filopodia are dynamic, actin-rich cellular protrusions that are important for processes such as cell migration, neuritogenesis, axon guidance, wound healing, angiogenesis, embryonic development, and phagocytosis (1, 2). Elucidating the exact mechanism(s) by which filopodia form will give a greater understanding of these cellular processes and how such structures play a role in pathological conditions such as metastasis (3) and pathogen invasion (4, 5). The Rho GTPase Cdc42 is a key regulator of cell signaling events that lead to filopodium formation in mammalian cells. It binds to and activates IRSp53 (insulin receptor substrate protein 53 kDa) (6–8). The Cdc42-IRSp53 complex induces filopodia by coupling membrane protrusion with actin dynamics (8). Interacting partners of IRSp53 include N-WASP (neural Wiskott-Aldrich syndrome protein) (8), Mena (mammalian enabled) (7, 9), Eps8 (EGF receptor kinase substrate 8) (10), and the Rac effectors WAVE (WASP family verprolin homology) isoforms WAVE1 (11–14) and WAVE2 (15). Yeast two-hybrid experiments have shown that IRSp53 binds mDia1 (mammalian Diaphanous 1) (16), but little else is known about this interaction.

mDia1 and mDia2 (mammalian Diaphanous 2) belong to the formin family of multidomain eukaryotic proteins that are involved in a wide range of cellular processes that require actin polymerization (17). Formins contain an actin-nucleating formin homology 2 domain, and a proline-rich, formin homology 1 domain that binds Src homology 3 and WW domain-containing proteins and profilin (18). Diaphanous-related formins, a subset of formins that bind to and are regulated by Rho GTPases, have additional domains flanking the formin homology 1 and formin homology 2 domains that enable signaling molecules to bind and exert control over formin protein conformation and functional state. These include an N-terminal GTPase binding domain, a Diaphanous inhibitory domain, and a C-terminal Diaphanous autoregulatory domain. Binding of Rho GTPases to the GTPase binding domain disrupts the autoinhibitory interaction between the Diaphanous autoregulatory domain and Diaphanous inhibitory domain, activating the Diaphanous-related formin (19). Recent findings also suggest that the Diaphanous-related formins mDia1 and mDia2 both contain a phospholipid-binding N-terminal basic domain that enables them to attach to the plasma membrane (20). mDia1 is a 140-kDa Diaphanous-related formin that forms stress fibers when activated by the Rho GTPase RhoA (21). This function of mDia1 is down-regulated by the protein phosphatase POPX2 (partner of PAK-interacting exchange factor 2), which binds to and inhibits activated mDia1 (22). Other roles of mDia1 include control of neurite outgrowth (23), cell polarity (24), and adherens junction integrity (25) downstream of RhoA and the assembly of the actin coat around endosomes under the control of RhoB (26). In addition, mDia1 stabilizes microtubules (27) and aligns them with actin filaments in the cell (28) and has been localized to the mitotic spindle (29).

The Rho GTPase Rif has been shown induce filopodia (30, 31). It shares only 32–49% identity with other Rho GTPases (30), and its N-terminal 19 residues bear no homology to other Rho family members apart from RhoD (32). Rif binds to the N-terminal region of both mDia1 and mDia2 *in vitro* (31, 33). Apart from these, no other interacting partners of Rif are known, and the signaling pathway(s) by which it drives the formation of actin-based cellular protrusions, such as filopodia, is poorly understood. In this study, we show by time lapse imaging

[S] The on-line version of this article (available at http://www.jbc.org) contains supplemental Figs. S1–S3 and Movies 1–8.

[1] Present address: Duke-NUS Graduate Medical School, 8 College Road, Singapore 169857.

[2] Present address: Florey Neurosciences Institutes, Parkville, Victoria 3010, Australia.

[3] To whom correspondence should be addressed. Tel.: 65-6407-0165; Fax: 65-6464-2049; E-mail: sohail.ahmed@imb.a-star.edu.sg.

of live cells that Rif drives the formation of dynamic filopodia with characteristics distinct from those of Cdc42-induced filopodia. Rif forms filopodia via a pathway that does not involve the Cdc42 effectors N-WASP and IRSp53 or the IRSp53 binding partner Mena. Furthermore, knockdown of the Rac effectors WAVE1 and WAVE2 does not disrupt Rif-mediated filopodia formation. Using acceptor photobleaching FRET (AP-FRET)[4] to examine Rif-mDia protein-protein interactions, we found that Rif interacts directly with mDia1 in filopodia but not with mDia2. mDia1 can by itself induce filopodia, and knocking it down inhibits Rif-driven filopodium formation. Taken together, these results suggest a novel pathway for filopodium formation via Rif and mDia1 that is independent of Cdc42 and Rac effectors.

EXPERIMENTAL PROCEDURES

Expression Constructs, Antibodies, and Reagents—pcDNA3-RifQL, pEF-Myc-mDia2, and pEF-Myc-mDia2H160D were from Harry Mellor (Bristol University, UK), pEYFP.C1-mDia1 was from Art Alberts (Van Andel Institute, Grand Rapids, MI, USA), pXJ40-GFP-actin was from Jingming Dong (GSK-Institute of Medical Biology, Singapore), p-mCherry-actin was from Maïté Coppey-Moisan (Institut Jacques Monod, Paris, France), and pIRESpuro3-mCherry-Abp140p was from Philippe Chavrier (Institut Curie, Centre de Recherche, Paris, France). pXJ40-mRFP-mDia1DN was constructed by cloning amino acids 771–1181 of mDia1 into the NotI and BglII sites of pXJ40-mRFP. The primary antibodies used were sheep polyclonal anti-Rif (1:400; from Harry Mellor), mouse monoclonal anti-IRSp53 (1:100 immunofluorescence, 1:1000 Western blot; from S. Ahmed), mouse monoclonal anti-mDia1 (610848, 1:500; BD Transduction Laboratories), rabbit polyclonal anti-mDia2 (N-terminal, 1:1000; from Shuh Narumiya, Kyoto University, Japan), rabbit polyclonal anti-HA (71–5500, 1:100; ZYMED), mouse monoclonal anti-tubulin (1:5000; Sigma), rabbit polyclonal anti-WAVE1 (W2142, 1:750; Sigma), rabbit polyclonal anti-WAVE2 (sc-33548, 1:250; Santa Cruz Biotechnology, Inc.), and HRP-conjugated mouse monoclonal anti-GAPDH antibody (G9295, 1:50,000; Sigma). The secondary antibodies used were Alexa Fluor™ 488 goat anti-mouse IgG (A11017, 1:400), Alexa Fluor™ 488 donkey anti-sheep IgG (A11015, 1:200), and Alexa Fluor™ 594 goat anti-rabbit IgG (A11037, 1:400), all from Molecular Probes, and HRP-conjugated goat anti-mouse IgG (sc-2005, 1:10,000), donkey anti-goat IgG (sc-2033, 1:2500), and goat anti-rabbit IgG (sc-2004, 1:5000), all from Santa Cruz Biotechnology, Inc. (Santa Cruz, CA). TRITC-conjugated phalloidin (1:1000) was from Sigma.

Cell Culture, Transfection, and Microinjection—N1E115, N-WASP WT and KO, and Mena WT and KO cells were cultured as described by Lim *et al.* (8). 293T cells were grown in DMEM supplemented with 4500 mg/liter glucose, 10% FBS, and 1% penicillin/streptomycin. All transient transfections were done according to the manufacturer's protocol using Lipofectamine 2000 (Invitrogen), except for IRSp53 siRNA, which was done using HiPerfect (Qiagen). Mena WT and KO cells were microinjected with cDNA as described by Lim *et al.* (8). For imaging experiments involving N1E115 cells, glass coverslips or glass bottom dishes were coated with 10 μg/ml laminin (Invitrogen).

Protein Knockdown by RNAi—Transient knockdown of proteins was done using the following siRNA oligonucleotides: IRSp53 (Stealth™ Select RNAi 1320003) from Invitrogen (8) and WAVE2 (sense 5′-GACGUUGCCUAGCGAUACAdTdT-3′) (34), mDia1 (sense 5′-GCUGGUCAGAGCCAUGGAU-3′) (23), and mDia2 (5′-AUAAGAGAGCAGUAUUUCAAA-3′) (35) from Sigma-Proligo. For transient knockdown of mouse WAVE1 protein, the following oligonucleotides and their respective reverse complements, separated by a 9-nucleotide hairpin spacer (TTCAAGAGA), were inserted into the pSuper expression vector: 5′-CGATGAGAAAGGCTTTCCG-3′ (pSuper-wave1) and 5′-CGCTATGAACGGTAGCTGA-3′ (non-targeting negative control pSuper-control). Decreases in target protein levels were assessed by Western blot of treated cells, and all calculations of percentage decrease were normalized for GAPDH or tubulin. In all RNAi experiments, only transfected cells were imaged and scored for filopodium formation. When the average transfection efficiency of 46.5% obtained using Lipofectamine 2000 for N1E115 cells[5] is taken into account, the actual level of knockdown attained in the population of cells analyzed is likely to be higher than estimated.

Immunofluorescence—Cells grown on glass coverslips were washed once with PBS, fixed with 4% paraformaldehyde in PBS for 30 min, and then washed twice with PBS for 10 min. Cells were then permeabilized with 0.5% (v/v) Triton X-100 in PBS for 1 min, washed twice with PBS for 10 min, and incubated with 3% BSA in PBS for 15 min. After treatment with primary antibodies at 37 °C for 1 h, cells were washed twice with PBST (PBS containing 0.1% Tween 20) for 10 min. Cells were next incubated with fluorescence-labeled secondary antibodies at 37 °C for 1 h and washed twice with PBST for 10 min and then once in PBS, and coverslips were mounted onto glass slides. All steps were carried out at room temperature unless otherwise specified. Cells were viewed using a fluorescence microscope (Zeiss Axiovert 200), and images were captured using a CoolSNAP CCD camera (Roper Scientific).

Live Cell Imaging—Cells grown in 35-mm diameter glass bottom dishes (Mattek) were placed on a 37 °C heated stage within a 5% CO_2 atmosphere chamber and imaged using a Zeiss Axiovert 200 fluorescence microscope enclosed within an incubator box, with a monochromator light source and a CoolSNAP CCD

[4] The abbreviations used are: AP-FRET, acceptor photobleaching FRET; % FE, percentage FRET efficiency; CC, correlation coefficient; TRITC, tetramethylrhodamine isothiocyanate; EYFP, enhanced yellow fluorescent protein; mRFP, monomeric red fluorescent protein; DIC, differential interference contrast.

[5] Average transfection efficiency obtained for N1E115 cells using Lipofectamine 2000 was 46.5%, as determined by transfecting cells with pXJ40-GFP vector and scoring for the percentage of GFP-positive cells in the entire population. In all RNAi experiments, knockdown efficiency was estimated by measuring the decrease in target protein level in the entire population of cells treated with RNAi, which includes untransfected cells. Only transfected cells were imaged and scored for filopodium formation. When the average transfection efficiency is taken into account, the actual level of knockdown attained in the population of cells analyzed is likely to be higher than estimated and in some cases could reach a maximum of 100%. However, we are unable to determine the exact percentage of knockdown.

camera (Roper Scientific). Images were captured in both differential interference contrast (DIC) and fluorescence channels at 10-s intervals over a 10-min time course, and movies were compiled using Metamorph software (Molecular Devices).

Analysis of Cell Morphology—For images of fixed cells, the following definitions of morphological characteristics were used. Peripheral projections were defined as thin, filopodia-like tubular protrusions arising from the cell periphery. Those of at least 5 μm in length were classified as long peripheral projections, and the rest were classified as short peripheral projections. Similar structures arising from the dorsal surface of the cell were defined as apical projections. Neurites were defined as linear peripheral protrusions of at least one cell body length. Neurites with structures such as short or long peripheral projections, ruffles, and/or lamellae emerging from along the neurite shaft were classified as complex neurites. Lamellae were defined as broad, flattened areas on the cell periphery that appeared to be completely adhered to the substrate. Similar structures that appeared loosely adherent were defined as ruffles. Ruffles were also observed to be able to fold back, and/or protrude from the dorsal surface of the cell. In each experiment, 10–20 cells were evaluated for the above morphological characteristics, and at least three independent experiments were carried out for any one set of conditions, giving a minimum n value of 30.

For time lapse imaging of live cells, filopodia were defined as dynamic, actin-containing tubular cell surface protrusions that could extend and retract. The number of filopodia/cell was determined by first marking out all filopodia-like structures that could be seen at the middle time point (*i.e.* the 31st image of a series of 61 captured over a 10-min time course) and then checking consecutive images taken before and after the middle time point, in both DIC and fluorescence channels. Only actin-positive structures for which both full extension and complete retraction could be observed in the series of consecutive images were scored as *bona fide* filopodia. Filopodial lifetime was measured starting from the initial appearance of the nascent structure up until the complete disappearance of the entire structure. Filopodial length was measured at the point of maximum extension. In each experiment, 3–10 cells were evaluated for the filopodial protrusion, and at least two independent experiments were carried out for any one set of conditions.

AP-FRET—AP-FRET was carried out using a Zeiss LSM 510 confocal microscope with a C-Apochromat 63X water 1.2 numerical aperture objective, with the following filter settings: for YFP, excitation source 514-nm laser line, dichroic mirror 458/514 nm, secondary dichroic mirror 515 nm, emission BP 530–600 nm; for mRFP, excitation source 561-nm laser line, dichroic mirror 405/488/561 nm, secondary dichroic mirror 565 nm, emission LP 575 nm. Regions of interest were selected, and the acceptor fluorophore (mRFP) was photobleached using 70% laser power and 50 iterations of the 561-nm laser line. The increase in donor fluorophore (EYFP) fluorescence intensity following mRFP bleaching was measured as FRET. FRET efficiency and cross-correlation values were calculated as described by Lim *et al.* (8). The combination of YFP as a donor with mRFP as the acceptor fluorophore has previously been used to measure FRET (36).

Statistical Analysis—Values in bar charts and tables are given as mean values ± S.E. unless otherwise indicated. Student's t test (two-tailed distribution, unpaired, equal variance) was calculated using Microsoft Excel, and the resulting p values are represented as follows: *, $p < 0.05$; **, $p < 0.01$; ***, $p < 0.001$.

RESULTS

Rif Phenotype in Neuronal Cells—The N1E115 mouse neuroblastoma cell line was used previously to measure the characteristics of filopodia induced by Cdc42 and its interacting partners IRSp53 and N-WASP (8). The typical morphology of untransfected N1E115 cells is shown in (Fig. 1*A*, *a*). To establish the phenotype of Rif in this cell line, N1E115 cells were transfected with a constitutively active mutant of Rif (RifQL) and stained with anti-Rif antibodies and TRITC-phalloidin at 18 h post-transfection. Rif induced apical filopodia-like projections at the dorsal surfaces of cells and filopodia-like peripheral projections at the cell edge (Fig. 1*A*, *b–d*). Complex neurites, lamellae (Fig. 1*A*, *c*), and ruffles (Fig. 1*A*, *d*) (see "Experimental Procedures" for definitions of various morphological structures) were also seen in a smaller percentage of transfected cells (Fig. 1*B*). All of these structures stained positive for Rif.

Rif Induces Filopodia in Neuronal Cells—Filopodia are highly dynamic, actin-rich, cylindrical membrane protrusions that extend and retract rapidly. They can also exhibit lateral motion and detach and lift up from the substratum (37). Many studies done on filopodia have been based on fixed cells, with no observation and quantification of the dynamics of the cellular structures in question (31, 38–42). Distinguishing true filopodia from protrusions that may appear similar under fixed conditions, such as retraction fibers and thin dendritic spines, is difficult at best. Quantitative data on *bona fide* filopodia can only be generated using time lapse analysis. In this study, we used the following approach to examine filopodia. Cells were cotransfected with GFP-actin and expression constructs of proteins of interest, and GFP-positive cells were observed in real time by high speed multichannel time lapse wide field imaging in both fluorescence and DIC channels. GFP-actin monomers were rapidly incorporated into the F-actin cytoskeleton, and dynamic actin-based cellular protrusions were thus marked by fluorescence and could be visualized and measured. Length, lifetime, and number of peripheral filopodia formed per cell were quantified as described by Lim *et al.* (8) and under "Experimental Procedures." Apical filopodia were not measured due to out-of-focus fluorescence making it impossible to define the full extent of the structures with two-dimensional imaging. In addition, the density of the apical filopodia formed and the fact that they could project at any angle relative to the cell surface and also bend meant that it was difficult to distinguish individual structures because many of them overlapped with one another.

To examine the dynamics of Rif-induced filopodia, N1E115 cells were cotransfected with GFP-actin and either untagged (Fig. 2*A*) or mRFP-tagged (Fig. 2*B*) RifQL and observed by time lapse imaging at 18 h post-transfection. The Rif-induced filopodia were dynamic structures (Fig. 2*A*) with an average length of 4.37 μm and average lifetime of 162 s (Table 1 and supplemental Movies 1 and 2). In contrast, the filopodia that formed in

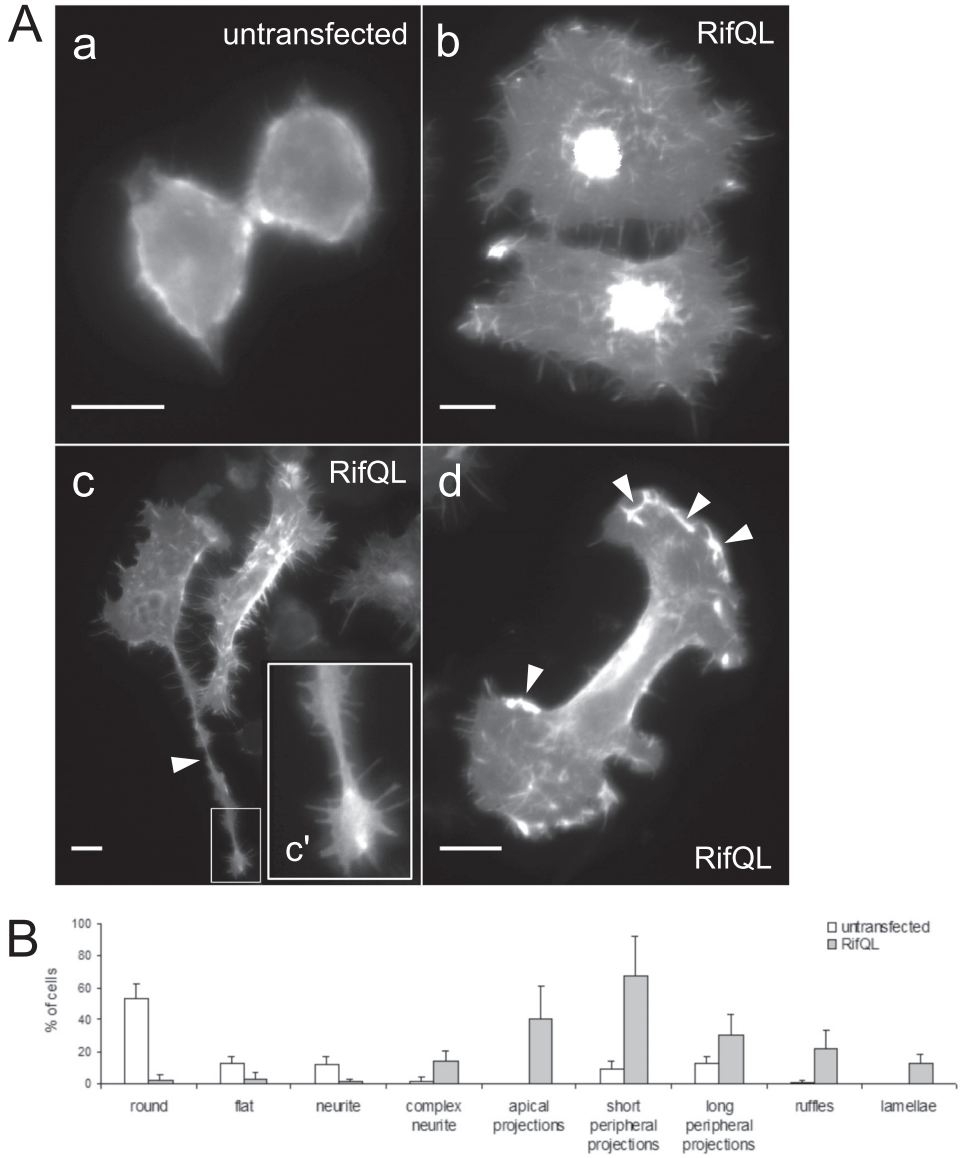

FIGURE 1. **Rif phenotype in neuronal cells.** *A*, *a*, Untransfected N1E115 cells were fixed and stained with TRITC-phalloidin. *b–d*, N1E115 cells were transfected with RifQL, fixed and stained with anti-Rif antibody. Examples of cells with apical and peripheral filopodia-like projections (*b–d*), complex neurite with filopodia-like projections and lamellae decorating the neurite shaft (*c*) (shown *magnified* in *c'*), and ruffles (*d*) (indicated by *arrowheads*) are shown. *Bar*, 10 μm. *B*, quantification of morphological characteristics of RifQL-overexpressing N1E115 cells described in *A*. Data are presented as mean ± S.E. (*error bars*) (untransfected, $n = 180$; RifQL, $n = 144$).

cells transfected with GFP-actin alone were longer (average length 7.09 μm) and fewer in number (Table 1). Rif-induced filopodia contained both actin and mRFP-Rif along their entire length (Fig. 2*B* and supplemental Movies 3–5). Longer Rif- and actin-positive protrusions were also seen in some of the transfected cells; however, they only extended, retracted, or remained static throughout the entire 10-min period of observation and thus did not fit our definition of filopodia. Many of these longer protrusions appeared at the trailing edge and lengthened as the cells retracted, and some were branched; these are likely to be retraction fibers.

Rif Does Not Require IRSp53 to Form Filopodia—We next set out to determine if Rif utilizes known effectors of Cdc42 and Rac to form filopodia. Cdc42 is believed to induce actin polymerization and filopodium formation through its downstream effectors, including N-WASP and IRSp53 (6–8, 43). RNAi, using a combination of three siRNA oligonucleotides targeting IRSp53, was used to determine if this protein is essential for Rif to form filopodia. Because these oligonucleotides were not efficiently transfected into N1E115 cells with Lipofectamine 2000, staggered transfections were done using two different transfection systems, with the siRNA oligonucleotides first introduced using HiPerfect, followed by plasmid DNA using Lipofectamine 2000 after a 4-h interval. To confirm the knockdown of IRSp53 by this method, N1E115 cells were transfected with IRSp53 siRNA or non-targeting negative control siRNA using HiPerfect at 0 h. At 4 h post-transfection, cells were then serum-starved for 5 h to simulate conditions of a second round of transfection using Lipofectamine 2000. Western blot of cell lysates probed using anti-IRSp53 antibodies showed a 63% decrease in IRSp53 protein level at 28 h post-transfection. (Note that if transfec-

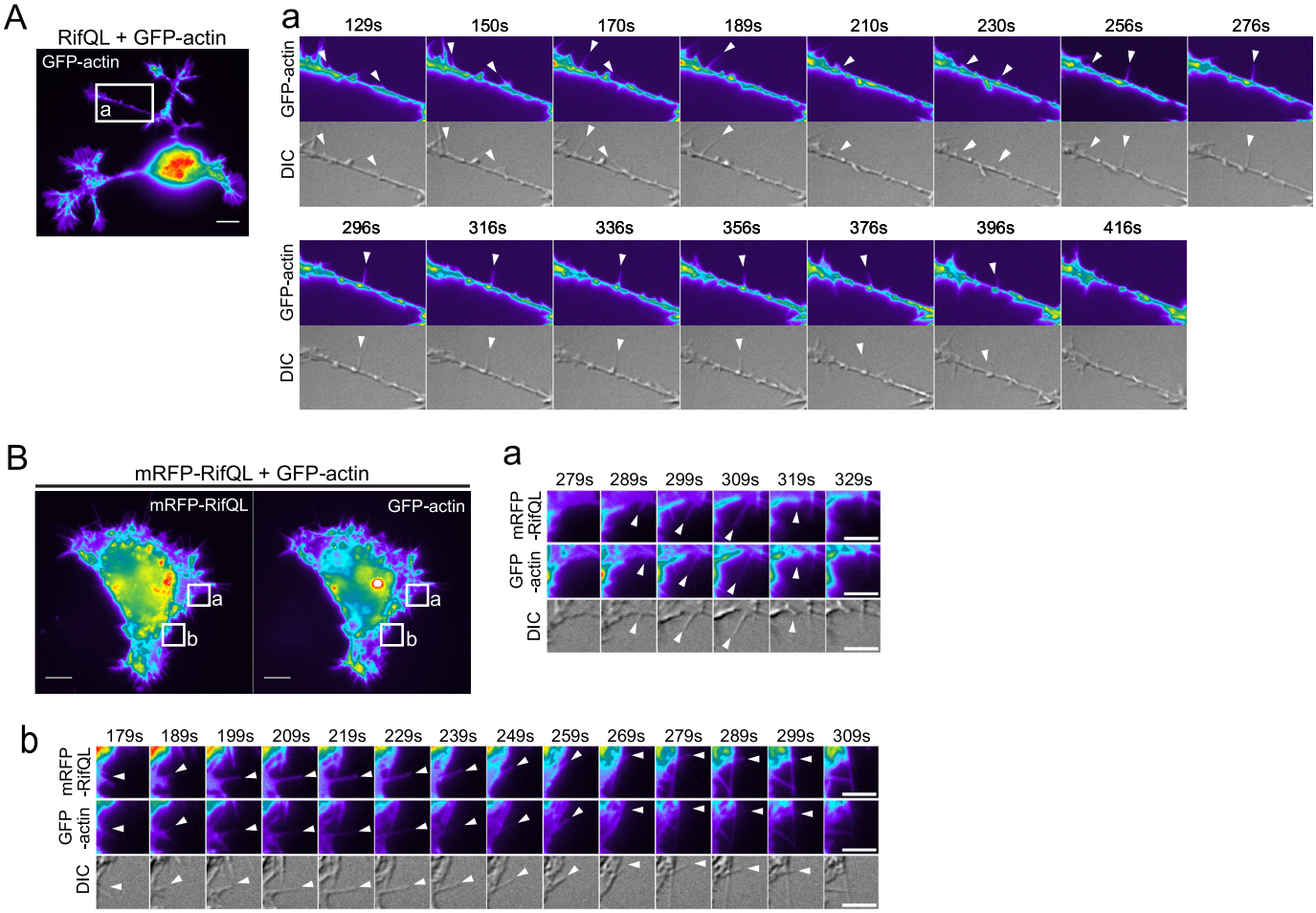

FIGURE 2. **Rif induces dynamic filopodia in neuronal cells.** *A*, N1E115 cells were cotransfected with RifQL and GFP-actin, and time lapse imaging of GFP-positive cells was done at 18 h post-transfection. *Bar*, 10 μm. *a*, a series of time lapse images of the *outlined* section of the cell, with *arrowheads* indicating individual filopodia (see supplemental Movies 1 and 2). *Bar*, 5 μm. *B*, N1E115 cells were cotransfected with mRFP-RifQL and GFP-actin, and time lapse imaging of cells expressing both mRFP and GFP was done at 18 h post-transfection. *Bar*, 10 μm. A series of time lapse images for both *outlined* sections of the cell are shown *magnified* in *a* and *b* (see supplemental Movies 3–5), with *arrowheads* indicating individual filopodia. *Bar*, 5 μm.

TABLE 1

Characteristics of filopodia induced by Rif and mDia1

N1E115 cells were cotransfected with cDNA for fluorescence-tagged actin or actin-binding peptide and the protein of interest. Time lapse imaging of fluorescent cells was done at 18 h post-transfection, and the number of filopodia formed per cell and the length and lifetime of such protrusions were measured (see "Experimental Procedures" for details). Endogenous, filopodia seen when cells were transfected with only GFP-actin; RifQL, cells cotransfected with untagged RifQL and GFP-actin; mDia1, cells cotransfected with EYFP-mDia1 and mCherry-Abp140p; mDia2, cells cotransfected with Myc-mDia2 and GFP-actin; mDia2H160D, cells cotransfected with Myc-mDia2H160D and GFP-actin; Rif + mDia2H160D, cells cotransfected with untagged RifQL, Myc-mDia2H160D, and GFP-actin. Data are presented as mean ± S.E. For endogenous, $n = 39$; RifQL, $n = 23$; mDia1, $n = 18$; mDia2, $n = 18$; mDia2H160D, $n = 20$; Rif + mDia2H160D, $n = 20$.

Protein(s) expressed	Filopodia/cell	Length	Lifetime
		μm	*s*
Endogenous	1.2 ± 1.02	7.16 ± 0.82	212 ± 64
IRSp53[a]		*6.80 ± 1.88*	*187 ± 38*
N-WASP[a]		*7.40 ± 0.97*	*154 ± 20*
RifQL	8.5 ± 2.36[b]	4.37 ± 0.28[c]	162 ± 14
mDia1	5.6 ± 1.27[d]	3.99 ± 0.60[c]	135 ± 19
mDia2	6.5 ± 0.73[b]	4.61 ± 1.76	163 ± 78
mDia2H160D	9.3 ± 2.61[b]	3.46 ± 0.12[d]	137 ± 42
Rif + mDia2H160D	7.0 ± 2.42[d]	3.35 ± 0.17[d]	135 ± 34

[a] Data for length and lifetime of IRSp53 and N-WASP filopodia in N1E115 cells from Lim *et al.* (8) are shown in italic type for comparison but excluded from the statistical analysis.
[b] $p < 0.001$ with respect to the values for "endogenous" in the same column.
[c] $p < 0.05$ with respect to the values for "endogenous" in the same column.
[d] $p < 0.01$ with respect to the values for "endogenous" in the same column.

tion efficiency is taken into account, the decrease in target protein levels in the cells examined for filopodium formation in all RNAi experiments in this study is likely to be higher than estimated by Western blot; see "Experimental Procedures" (Fig. 3*A*).[5]) To confirm knockdown of IRSp53 at the phenotype level, the same protocol was used to introduce IRSp53 or control siRNA followed by HA-tagged N-WASP cDNA into N1E115 cells. Cells were fixed and stained with anti-HA antibody 28 h after the first set of transfections and imaged. IRSp53 is believed to synergize with N-WASP to induce neurite outgrowth because it drives the formation of neurites in N-WASP WT but not N-WASP KO cells (8). Here, a decrease in neurite outgrowth in HA-positive N1E115 cells treated with IRSp53 siRNA was observed, indicating that the reduction in IRSp53 expression attained by this method was enough to disrupt the cytoskeletal phenotype of IRSp53 (Fig. 3*B*). Staggered transfections of N1E115 cells were then carried out to determine if IRSp53 knockdown affects Rif-induced filopodium formation. RifQL formed the same ($p > 0.05$) average number of filopodia per cell in both IRSp53 and negative control siRNA-treated cells, and the structures were of similar lengths (Fig. 3*C* and Table 2).

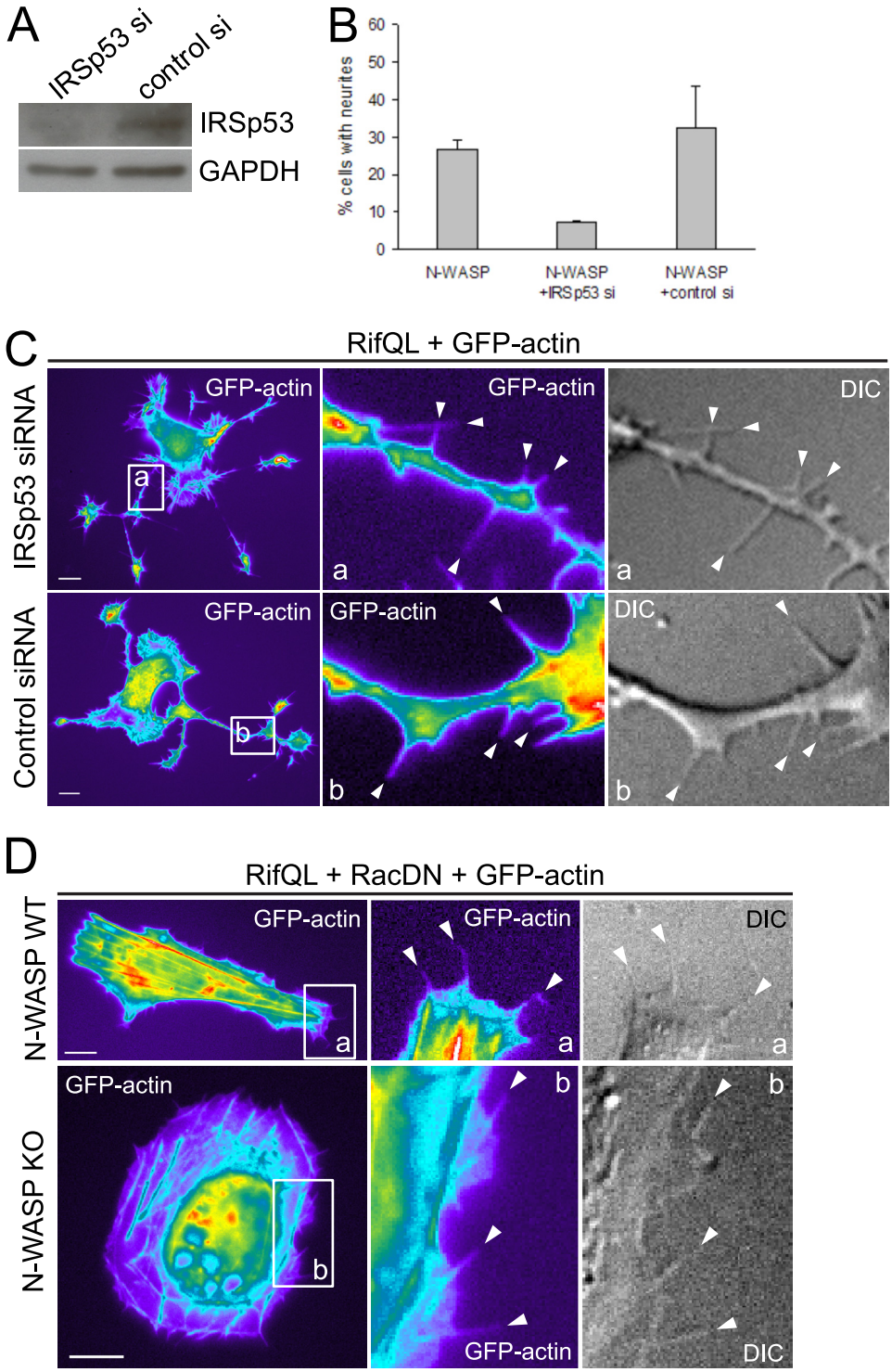

FIGURE 3. **Rif does not require IRSp53 or N-WASP to form filopodia.** *A*, Western blot showing IRSp53 protein levels N1E115 cells 28 h after transfection with IRSp53 or non-targeting control siRNA. Cells were first transfected with IRSp53 or control siRNA using HiPerfect. At 4 h post-transfection, cells were serum-starved for 5 h to simulate subsequent transfection using Lipofectamine 2000 (see "Experimental Procedures"), as would be done in live cell imaging experiments. Cells were then harvested at the 28 h time point. *B*, N1E115 cells were first transfected with either IRSp53 or control siRNA using HiPerfect and 4 h later with HA-N-WASP cDNA using Lipofectamine 2000. Cells were then fixed and stained with anti-HA antibody 28 h after the first round of transfection, and the percentage of HA-positive cells with neurites was scored. *C*, sequential transfections of N1E115 cells with IRSp53 or control siRNA and then RifQL and GFP-actin cDNA were carried out. At 28 h after the first round of transfection, time lapse imaging of GFP-positive cells was done. *Bar*, 10 μm. *Magnified* sections of transfected cells are shown in *a* and *b*, with *arrowheads* indicating individual filopodia. *D*, N-WASP WT and KO cells were cotransfected with RifQL, RacDN, and GFP-actin. Time lapse imaging of GFP-positive cells was done at 18 h post-transfection. *Bar*, 10 μm. *Magnified* sections of transfected cells are shown in *a* and *b*, with *arrowheads* indicating individual filopodia. *Error bars*, S.E.

Rif Does Not Require N-WASP to Form Filopodia—N-WASP WT and KO cells were cotransfected with RifQL and GFP-actin to determine if Rif requires N-WASP to form filopodia. Membrane ruffling that could potentially obscure any filopodia formed was observed in both N-WASP WT and KO cells (supplemental Fig. S1*A*), and an average of about two filopodia per

TABLE 2

Effect of Cdc42 and Rac effector knockdown on Rif-driven filopodium formation

RNAi, N1E115 cells were transfected with RifQL, GFP-actin, and RNAi targeting the protein of interest or non-targeting control RNAi, and time lapse imaging was done on GFP-positive cells. KO, N-WASP KO and WT cells were transfected with RifQL, RacDN, and GFP-actin, and time lapse imaging was done on GFP-positive cells. DN, N1E115 cells were transfected with RifQL, mRFP-mDia1DN, and GFP-actin, and time lapse imaging was done on cells positive for both GFP and mRFP. For control cells, mRFP-mDia1DN was omitted, and GFP-positive cells were imaged. The number of filopodia formed per cell and the length and lifetime of such protrusions were measured (see "Experimental Procedures" for details). Data are presented as mean ± S.E. For IRSp53 siRNA, $n = 33$; control siRNA, $n = 32$; WAVE1 shRNA, $n = 19$; control shRNA, $n = 20$; WAVE2 siRNA, $n = 10$; control siRNA, $n = 18$; mDia1 siRNA, $n = 19$; control siRNA, $n = 20$; mDia2 siRNA, $n = 28$; control siRNA, $n = 18$; N-WASP KO, $n = 20$; N-WASP WT, $n = 21$; mDia1DN, $n = 29$; control, $n = 23$).

KD, KO, or dominant negative	Filopodia/cell	Length	Lifetime
		μm	*s*
RNAi			
IRSp53 siRNA	9.4 ± 1.18	4.11 ± 0.27	138 ± 23
Control siRNA	9.2 ± 3.82	3.74 ± 0.31	108 ± 14
WAVE1 shRNA	11.8 ± 3.27	5.01 ± 1.34	153 ± 72
Control shRNA	10.8 ± 1.07	5.31 ± 0.64	136 ± 21
WAVE2 siRNA	10.0 ± 3.07	3.61 ± 0.24	131 ± 20
Control siRNA	15.0 ± 3.81	4.19 ± 0.41	121 ± 20
mDia1 siRNA	6.1 ± 1.99[a]	3.76 ± 0.29	109 ± 38
Control siRNA	11.4 ± 3.36	4.00 ± 0.79	146 ± 33
mDia2 siRNA	3.0 ± 1.24[b]	3.86 ± 0.33	123 ± 24
Control siRNA	7.7 ± 0.85	4.05 ± 0.26	109 ± 16
KO			
N-WASP KO	10.0 ± 1.96	3.26 ± 1.19	155 ± 49
N-WASP WT	8.9 ± 1.94	3.19 ± 0.60	202 ± 53
Dominant negative			
mDia1DN	3.4 ± 1.63[a]	3.34 ± 0.21	130 ± 48
Control	8.5 ± 2.36	4.37 ± 0.28	162 ± 14

[a] $p < 0.05$ compared with control.
[b] $p < 0.01$ compared with control.

cell was recorded for both WT and KO cells (supplemental Fig. S1*B*). When dominant negative Rac1 (RacDN) was cotransfected with RifQL and GFP-actin, membrane ruffling was suppressed, and the average number of filopodia/cell rose to 8–10 (Fig. 3*D* and supplemental Fig. S1*B*). RacDN co-expressed with GFP-actin in the absence of RifQL did not induce any significant filopodial protrusion (supplemental Fig. S1*B*), confirming that the increase in filopodia number was a direct result of Rif activity rather than RacDN. There was no statistically significant difference ($p > 0.05$) in the number of filopodia formed per cell and in the average length and lifetime of filopodia formed between N-WASP WT and KO cells (Fig. 3*C* and Table 2). Furthermore, the fact that RacDN could suppress RifQL-induced membrane ruffling suggests that Rif might act through Rac1 to induce ruffling in fibroblasts.

Rif Does Not Require Mena to Form Filopodia—Mena is an IRSp53 interactor (7) that localizes to the tips of filopodia (9). IRSp53 is unable to form filopodia in Mena KO cells, demonstrating that this protein is essential to the Cdc42-IRSp53 pathway for filopodium formation (8). Mena KO cells were microinjected with RifQL and GFP-actin plasmid DNA to establish if Rif requires Mena in order to form filopodia. Because the Mena WT cell line had been created from Mena KO cells by stable transfection with GFP-tagged Mena, mCherry-actin cDNA was used in place of GFP-actin cDNA to visualize actin within cellular structures. RifQL was able to induce filopodial protrusion in both Mena WT and KO cells (supplemental Fig. S2) as early as 2 h postinjection.

Rif Does Not Require WAVE1 to Form Filopodia—The Rac effector WAVE1 binds to the Src homology 3 domain of IRSp53 *in vitro* (8) and has been reported to be in the filopodia of spreading platelets (11), early stage oligodendrocyte precursor cells (12), and hippocampal neuron growth cones (13). The shRNA plasmid vectors pSuper-wave1 and pSuper-control were used to test if Rif-induced filopodium formation requires WAVE1. Western blot of cell lysates probed using anti-WAVE1 antibodies showed a 97% decrease in WAVE1 protein level at 36 h post-transfection (Fig. 4*A*).[5] N1E115 cells were subsequently cotransfected with RifQL, GFP-actin, and pSuper-wave1 or -control using the same protocol and observed by time lapse imaging. Rif was able to drive filopodium formation in both pSuper-wave1- and pSuper-control-treated cells (Fig. 4*C*), and there was no statistically significant difference ($p > 0.05$) in the number of filopodia formed per cell, filopodial length, and filopodial lifetime between the experimental and control set-ups (Table 2).

Rif Does Not Require WAVE2 to Form Filopodia—WAVE2 interacts with the Src homology 3 domain of IRSp53 in T cells (8) and colocalizes with IRSp53 at filopodial tips in melanoma cells (15). To establish if Rif uses WAVE2 to form filopodia, N1E115 cells were treated with siRNA targeting WAVE2. Western blot of cell lysates probed using anti-WAVE2 antibodies showed a 66% decrease in WAVE2 protein level at 42 h post-transfection (Fig. 4*B*).[5] N1E115 cells were subsequently transfected with WAVE2 or control siRNA and 22 h later with RifQL and GFP-actin, and they were observed at 42 h after the first round of transfection by time lapse imaging. Rif was able to drive filopodium formation in both WAVE2- and control siRNA-treated cells (Fig. 4*D*), and there was no statistically significant difference ($p > 0.05$) in the number of filopodia formed per cell, filopodial length, and filopodial lifetime between the experimental and control set-ups (Table 2).

Rif-mediated Filopodium Formation in N1E115 Cells Involves both mDia1 and mDia2—Rif has been proposed to drive a Cdc42-independent pathway of filopodium formation using mDia2 as an effector in fibroblasts (31). However, mDia2 itself has also been proposed to form filopodia downstream of Cdc42 (38). To see if Rif and mDia2 are able to work together to drive filopodia in N1E115 cells, cells cotransfected with RifQL, Myc-mDia2H160D, and GFP-actin were observed by time lapse microscopy. mDia2H160D contains a point mutation that renders it unable to interact with Cdc42 (38) while still retaining its ability to bind Rif (31), and changes in filopodial protrusion seen in cells transfected with this mutant would thus be attributed to its interaction with Rif rather than with Cdc42. Cells cotransfected with mDia2H160D and GFP-actin were able to form filopodia with characteristics similar to that of Rif filopodia (Table 1). This demonstrates that mDia2 is capable of driving filopodium formation independently of Cdc42. However, when cells were cotransfected with both RifQL and mDia2H160D, there was no increase in average filopodia number, length, or lifetime (Table 1) over the corresponding values obtained by transfecting either RifQL or mDia2H160D alone.

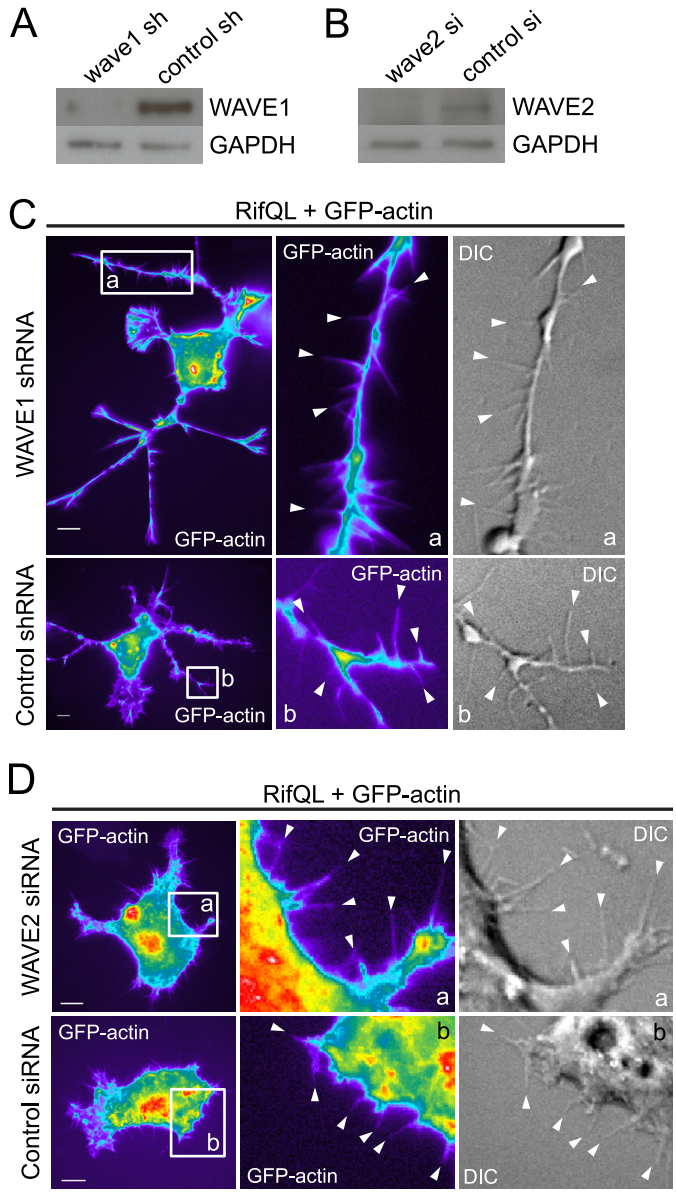

FIGURE 4. **Rif does not require WAVE1 or WAVE2 to form filopodia.** *A*, Western blot showing WAVE1 protein levels in N1E115 cells 36 h after transfection with WAVE1 or non-targeting control shRNA. *B*, Western blot showing WAVE2 protein levels in N1E115 cells 42 h after transfection with WAVE2 or non-targeting control siRNA. *C*, N1E115 cells were cotransfected with RifQL, GFP-actin, and either WAVE1 or control shRNA. Time lapse imaging of GFP-positive cells was done at 36 h post-transfection. *Bar*, 10 μm. *Magnified* sections of transfected cells are shown in *a* and *b*, with *arrowheads* indicating individual filopodia. *D*, N1E115 cells were transfected with RifQL, GFP-actin, and either WAVE2 or control siRNA. Time lapse imaging of GFP-positive cells was done at 42 h post-transfection. *Bar*, 10 μm. *Magnified* sections of transfected cells are shown in *a* and *b*, with *arrowheads* indicating individual filopodia.

This is in contrast to what would be expected if the two proteins did indeed synergize. For comparison, data from cells cotransfected with Myc-tagged wild type mDia2 and GFP-actin are included (Table 1).

Next, we tested the effect of an mRFP-tagged dominant negative mutant of mDia1 (mRFP-mDia1DN) on Rif filopodia. This mutant has been previously shown to inhibit both mDia1 and mDia2 function (44). N1E115 cells were cotransfected with RifQL, mRFP-mDia1DN, and GFP-actin, and cells positive for both GFP and mRFP were observed by time lapse imaging at 18 h post-transfection. There was a statistically significant reduction ($p < 0.05$) in the number of filopodia formed per cell in the presence of mRFP-mDia1DN (Fig. 5*A* and Table 2). To confirm and extend the results obtained with mRFP-mDia1DN, we knocked down mDia1 and mDia2 separately to determine which isoform is involved in Rif-mediated filopodium formation.

Lysates were obtained from N1E115 cells treated with mDia2 siRNA at 40 h post-transfection and analyzed by Western blot using an antibody specific for mDia2, as confirmed by its ability to detect overexpressed EYFP-mDia2 (supplemental Fig. S3). An 87% decrease in mDia2 protein level was seen (Fig. 5*B*).[5] N1E115 cells were then cotransfected with RifQL, mDia2, or control siRNA and GFP-actin, and GFP-positive cells were observed by time lapse imaging at 40 h post-transfection. Although the average length and lifetime of filopodia formed were similar, there was a statistically significant decrease ($p < 0.01$) in the number of filopodia formed per cell when mDia2 was knocked down (Fig. 5*D* and Table 2). Similar results were observed when mDia2 was knocked down in N-WASP WT, a cell line in which we have shown Rif to be capable of inducing filopodia. Western blots of lysates from N-WASP WT cells transfected twice with mDia2 siRNA (with a 20-h interval between the two rounds of transfection) showed a 98% decrease in mDia2 protein expression at 44 h after the first round of transfection. There was a statistically significant decrease ($p < 0.01$) in the number of filopodia formed per cell from 7.8 ± 0.73 (control) to 1.8 ± 0.85 (mDia2 knockdown) when mDia2 was silenced.

Western blots of lysates from cells treated with mDia1 siRNA showed an 81% decrease in mDia1 protein level at 24 h post-transfection (Fig. 5*C*).[5] N1E115 cells were then cotransfected with RifQL, mDia1, or control siRNA and GFP-actin, and GFP-positive cells were observed by time lapse imaging at 24 h post-transfection. Similar to the results obtained by knocking down mDia2, a statistically significant decrease ($p < 0.05$) in the number of filopodia formed per cell was also seen when mDia1 was silenced (Fig. 5*E* and Table 2), whereas the average length and lifetime of filopodia formed did not differ. Further evidence for a role for mDia1 in filopodium formation was derived by overexpressing EYFP-mDia1 in N1E115 cells. In this experiment, pIRESpuro3-mCherry-Abp140p, which encodes an mCherry-tagged *Saccharomyces cerevisiae* F-actin-binding peptide (45), was cotransfected as a label for endogenous F-actin. EYFP- and mCherry-positive cells were observed by time lapse imaging at 18 h post-transfection. EYFP-mDia1 triggered the protrusion of filopodia that were positive for both EYFP and mCherry along their lengths (Fig. 6 and supplemental Movies 6–8), showing that they contained both mDia1 and actin. The average length (3.99 μm) and lifetime (135 s) of the mDia1 filopodia were similar to that of Rif filopodia ($p > 0.05$). As was the case for Rif filopodia, mDia1 filopodia were also shorter than endogenous ones ($p < 0.05$) as well as those induced by IRSp53 and N-WASP (Table 1).

Rif Interacts with mDia1 but Not mDia2 in Filopodia—We have previously used AP-FRET to show protein-protein interaction in filopodia (8, 46, 47). To determine if Rif interacts with

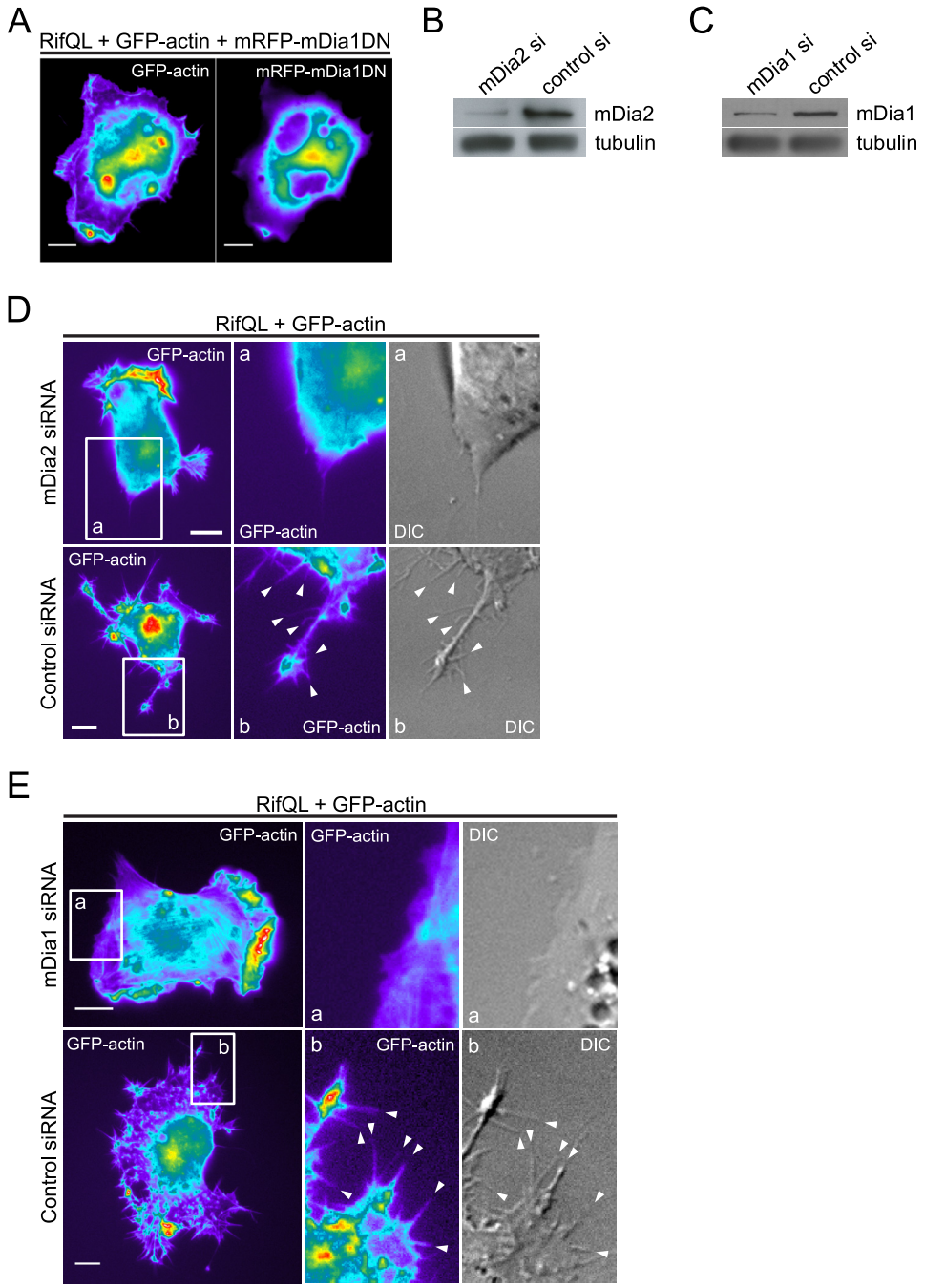

FIGURE 5. **Rif filopodium formation involves mDia1 and mDia2.** *A*, N1E115 cells were cotransfected with RifQL, mRFP-mDia1DN, and GFP-actin, and time lapse imaging of cells expressing both mRFP and GFP was done at 18 h post-transfection. *Bar*, 10 μm. *B*, Western blot showing mDia2 protein levels in N1E115 cells 40 h after transfection with mDia2 or non-targeting control siRNA. *C*, Western blot showing mDia1 protein levels in N1E115 cells 24 h after transfection with mDia1 or non-targeting control siRNA. *D*, N1E115 cells were cotransfected with RifQL, GFP-actin, and either mDia2 or non-targeting control siRNA, and time lapse imaging of GFP-positive cells was done at 40 h post-transfection. *Bar*, 10 μm. *Magnified* sections of transfected cells are shown in *a* and *b*, with *arrowheads* indicating individual filopodia. *E*, N1E115 cells were cotransfected with RifQL, GFP-actin, and either mDia1 or non-targeting control siRNA, and time lapse imaging of GFP-positive cells was done at 24 h post-transfection. *Bar*, 10 μm. *Magnified* sections of transfected cells are shown in *a* and *b*, with *arrowheads* indicating individual filopodia.

mDia1 or mDia2 in filopodia, a similar approach was used here. N1E115 cells were cotransfected with mRFP-RifQL and EYFP-mDia1 or -mDia2 and fixed at 24 h post-transfection. mRFP-RifQL (acceptor) was bleached in selected regions of interest, and resultant changes in EYFP-mDia1 or -mDia2 (donor) and acceptor fluorescence were measured. FRET occurs when donor and acceptor molecules are no further than 10 nm apart and is expressed in terms of percentage of FRET efficiency (% FE). FRET also gives rise to a negative correlation in the rates of change of fluorescence between the acceptor and donor, which is quantified and expressed as a correlation coefficient (CC) (8). Three controls were used: a positive control tandem mRFP-EYFP construct and the negative control pairs mRFP with EYFP-mDia1 and mRFP with EYFP-mDia2. Positive control FRET had an average % FE value of 17.8% and an average CC of −0.97, whereas that of the negative controls ranged from 1.4 to

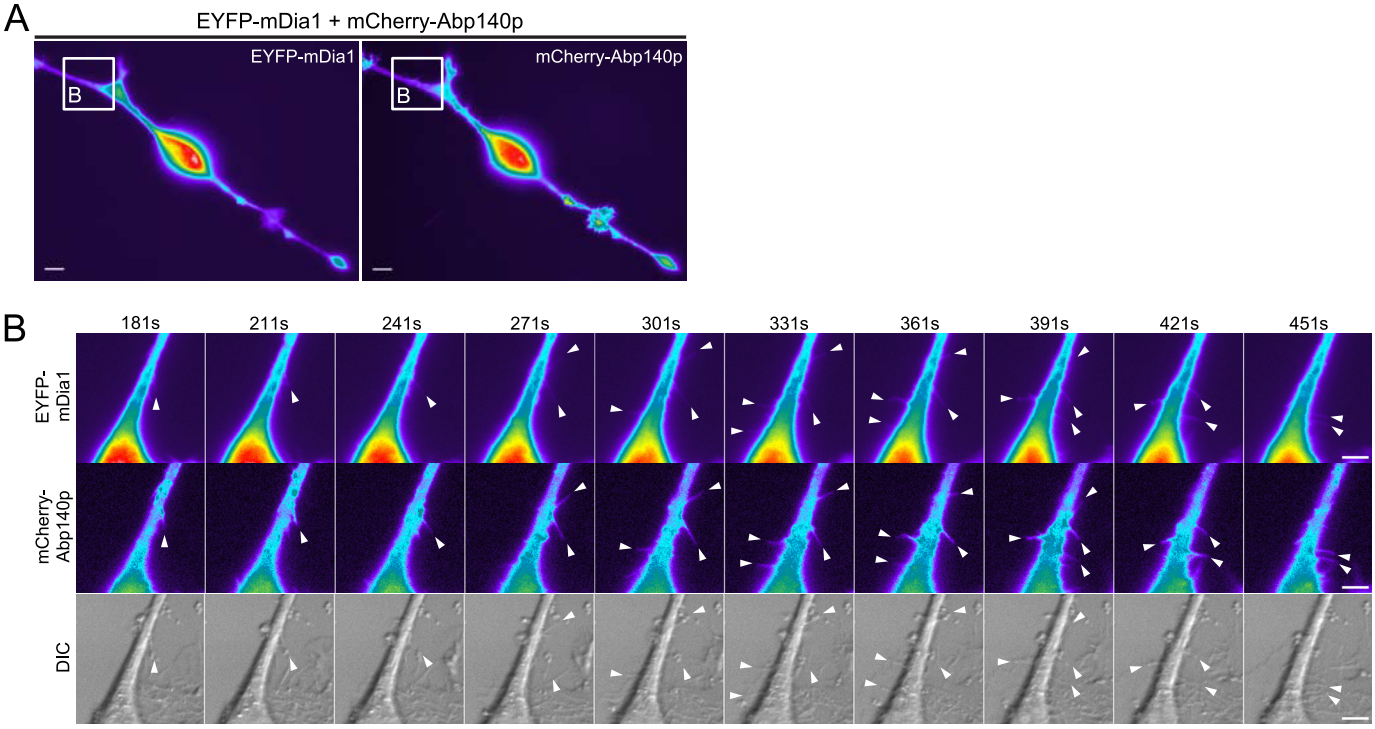

FIGURE 6. **mDia1 induces filopodia in neuronal cells.** *A*, N1E115 cells were cotransfected with EYFP-mDia1 and mCherry-Abp140p, and time lapse imaging of cells expressing both EYFP and mCherry was done at 20 h post-transfection. *B*, the series of time lapse images shows a section of the transfected cell in *A*, with *arrowheads* indicating individual filopodia (see supplemental Movies 6–8). *Bar*, 5 μm.

4.0% and from 0.05 to −0.41, respectively (Fig. 7*A* and Table 3). % FE values greater than 3% with corresponding CC values of −1.0 to −0.7 were taken as an indication of positive FRET and protein-protein interaction. Positive FRET between RifQL and mDia1 was observed in both filopodia-like projections (Fig. 7*B*, *a* and *c*) and ruffles (Fig. 7*B*, *b*), showing that RifQL interacts with mDia1 in these structures *in vivo* (Table 3). In contrast, although the filopodia-like projections of cells coexpressing mRFP-RifQL and EYFP-mDia2 were positive for both proteins, FRET was not detected between them (Fig. 7*C*, *a*), and it is likely that these two proteins do not interact, at least within these structures as well as at the cell edge (Fig. 7*C* (*b*) and Table 3).

DISCUSSION

Characteristics of Rif Filopodia—Observations of fixed cells have formed the basis of many studies done on filopodia (31, 38–42); however, with this approach, it is not possible to observe the movement that characterizes and defines filopodia as dynamic structures. Studying these protrusions in live cells is a definitive way of distinguishing them from static retraction fibers and thin dendritic spines because all three types of protrusions contain actin and are thin and cylindrical, thus appearing similar in fixed cells. Time lapse observations are also essential for quantitative analysis of filopodium formation and investigating the cell signaling pathways involved. Although some groups have examined filopodia in live cells by time lapse microscopy, structures that remained stationary (48) or went through only extension or retraction phases but not both processes (49–51) were all scored for. In other time lapse studies, the actin content of filopodia-like protrusions was either not monitored at all or detected by F-actin staining after the end of the time lapse observations rather than simultaneously (52–55). This lack of a standard definition of filopodia makes it difficult to compare results across various studies performed under different experimental conditions. Moreover, the I-BAR (inverse bin-amphiphysin-Rvs) domain of IRSp53 (8) and the F-BAR (Fes/CIP4 homology bin-amphiphysin-Rvs) domain of srGAP2 (slit-robo GTPase-activating protein 2) (56) have both been found to be capable of producing filopodia-like protrusions that do not contain actin, highlighting the importance of tracking the actin content of such structures in order to confirm whether they are indeed true filopodia.

Rif was first shown to be an inducer of filopodia in HeLa and NIH3T3 cells (30, 31). However, in those studies, the Rif signaling pathway to filopodium formation was investigated using fixed cells (30, 31). In this study on Rif, we used the definition of filopodia and method of measurement proposed by Lim *et al.* (8) to track the life history of filopodia containing microfilaments tagged with GFP-actin or mCherry-Abp140p in live cells by high speed sequential multichannel time lapse imaging. With this method, we were able to observe the dynamics of filopodia in real time, verify their actin content, and quantify their length and lifetime. Only structures that were observed to fully extend and then completely retract were taken into account. Under this set of criteria, Rif was found to drive the formation of peripheral filopodia in N1E115 cells with an average length significantly shorter than that of the endogenous ones (7.16 μm), which are similar in length to those induced by the key Cdc42 effectors IRSp53 (6.80 μm) and N-WASP (7.40 μm) in the same cell line (8). This is in contrast to the previous observation that Rif filopodia are longer than those formed by

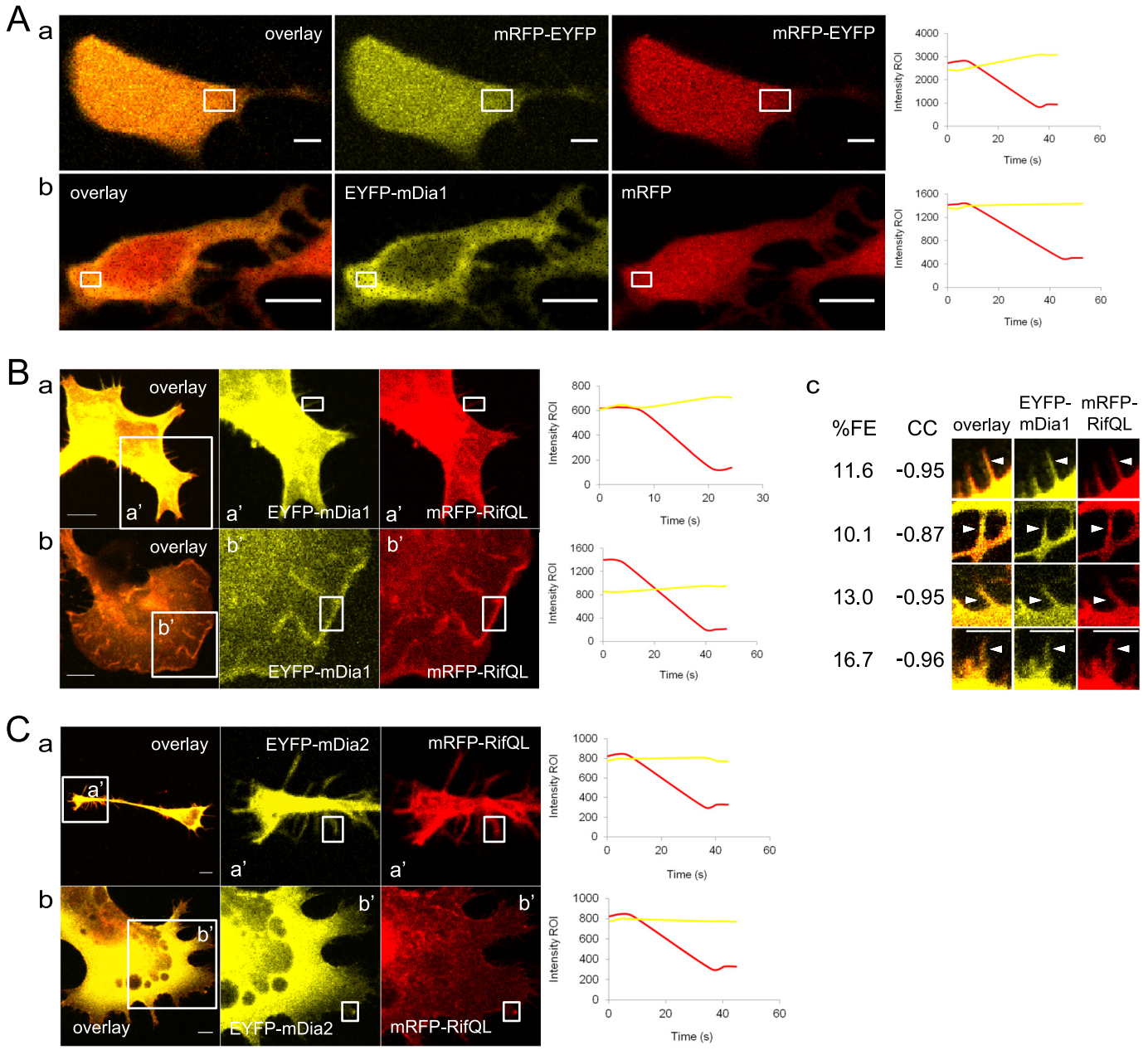

FIGURE 7. **Rif interacts with mDia1 but not mDia2 in filopodia.** N1E115 cells transfected with tandem mRFP-EYFP (positive control) (*A*, *a*), mRFP and EYFP-mDia1 (negative control) (*A*, *b*), mRFP-RifQL and EYFP-mDia1 (*B*), or mRFP-RifQL and EYFP-mDia2 (*C*) were fixed at 24 h post-transfection. Fluorescence intensities of selected regions of interest were monitored in both mRFP and EYFP channels for the entire duration of the experiment. mRFP was bleached using a 561-nm laser once base-line intensities of both mRFP (acceptor) and EYFP (donor) fluorescence were established. Subsequent changes in these fluorescence intensities were measured and expressed as % FE, and the correlation between the rates of change of these values was expressed as CC (see "Experimental Procedures" for details). % FE and CC values obtained for the various control and experimental set-ups are given in Table 3. Positive FRET was defined as % FE of >3% with CC values of −1.0 to −0.7. Regions of interest used for FRET measurements are *outlined* in *white* in *A*, *B* (*a'* and *b'*), and *C* (*a'* and *b'*). The *arrowheads* indicate individual filopodia used for FRET measurements (*B*, *c*). *Bar*, 5 μm.

Cdc42 (31). In that study, observations were done on fixed cells, and actual measurements of filopodial length were not reported. In the time lapse observations of Rif-induced filopodia done by Ellis and Mellor (30), filopodia were not clearly defined by characteristics such as length and lifetime. In our time lapse studies, longer static mRFP- and GFP-positive filopodia-like structures were seen in addition to the shorter dynamic filopodia in cells coexpressing mRFP-RifQL and GFP-actin. However, these longer protrusions remained stationary throughout or were observed to only either extend or retract during the 10-min period of observation, and some of them were branched. Retraction fibers left behind as cells contracted and/or neurites collapsed were also positive for both mRFP-RifQL and GFP-actin. These observations with mRFP-RifQL indicate that Rif is present not only in filopodia but in retraction fibers as well and might explain the disparity in conclusions drawn on the length of Rif filopodia in this study and previous ones that were done using fixed cells.

Rif Forms Ruffles and Lamellae—In this study, Rif was found to drive not just apical and peripheral filopodia in neuronal cells

TABLE 3

FRET analysis of Rif-mDia1 interaction

N1E115 cells transfected with controls, mRFP-RifQL and EYFP-mDia1, or mRFP-RifQL and EYFP-mDia2 were fixed at 24 h post-transfection. Fluorescence intensities of selected regions of interest were monitored in both mRFP and EYFP channels for the entire duration of the experiment. mRFP was bleached using a 561-nm laser once base-line intensities of both mRFP (acceptor) and EYFP (donor) fluorescence were established. Subsequent changes in these fluorescence intensities were measured and expressed as % FE, and the correlation between the rates of change of these values is expressed as CC (see "Experimental Procedures" for details). Positive FRET was defined as % FE > 3% with CC values of −1.0 to −0.7. Data are presented as mean ± S.D. (for mRFP-EYFP, $n = 14$; mRFP/EYFP-mDia1, $n = 7$; mRFP/EYFP-mDia2, $n = 6$; mRFP-RifQL/EYFP-mDia1 in filopodia-like projections, $n = 9$; mRFP-RifQL/EYFP-mDia1 in ruffles, $n = 7$; mRFP-RifQL/EYFP-mDia2 in filopodia-like projections, $n = 5$; mRFP-RifQL/EYFP-mDia2 in cell edge, $n = 5$).

FRET pairs	% FE	CC
Controls		
mRFP-EYFP (tandem positive control)	17.8 ± 3.6	−0.97 ± 0.04
mRFP and EYFP-mDia1 (negative control)	4.0 ± 2.3	−0.41 ± 0.42
mRFP and EYFP-mDia2 (negative control)	1.4 ± 1.7	0.05 ± 0.37
Rif and mDia1		
mRFP-RifQL and EYFP-mDia1 (filopodia)	11.3 ± 5.0	−0.94 ± 0.07
mRFP-RifQL and EYFP-mDia1 (ruffles)	11.7 ± 3.4	−0.95 ± 0.04
Rif and mDia2		
mRFP-RifQL and EYFP-mDia2 (filopodia)	4.8 ± 5.0	−0.18 ± 0.45
mRFP-RifQL and EYFP-mDia2 (cell edge)	2.8 ± 4.7	−0.11 ± 0.50

but membrane ruffles and lamellae as well. In N-WASP WT and KO fibroblasts, Rif induced peripheral membrane ruffling that was blocked by coexpression of dominant negative Rac. Little is known about Rif effectors and how any of them might be linked to activation of Rac, so it remains to be seen how Rif might, like Cdc42 (57), function upstream of Rac in triggering such cytoskeletal changes. It would also be interesting to test if exogenous WAVE1 or WAVE2 is able to rescue RacDN inhibition of Rif ruffling in N-WASP WT and KO cells. Our FRET studies also show that Rif and mDia1 interact with each other in ruffles. Although mDia1 has been reported to localize to membrane ruffles in both epithelial carcinoma (58) and Jurkat cells, and mDia1 KO T cells have been found to be defective in ruffle formation (59), how exactly mDia1 contributes to the protrusion of these structures is not known.

Rif Does Not Require Cdc42 or Rac Effectors to Form Filopodia—Apart from mDia1 (33) and mDia2 (31), no other interacting partners of Rif are known, and the signaling pathway by which it drives actin-based cellular protrusions is poorly understood. Rif has been linked to filopodia through mDia2 via a pathway that appears to exclude both Cdc42 and Arp2/3 complex, based on evidence from fixed cells (31). However, the question of whether Rif and mDia2 are truly involved in a distinct pathway remained unresolved because the possible involvement of Cdc42 effectors, such as N-WASP, IRSp53, and the IRSp53 binding partner Mena, had yet to be investigated and ruled out. mDia2 itself has previously been put forward as an effector of Cdc42 in filopodium formation (38). In this study, a combination of RNA interference and knock-out cell lines was used to establish that Rif forms filopodia without the need for various key effectors of Cdc42 and Rac and is thus likely to helm a distinct pathway for filopodium formation. Rif was able to drive filopodia in N-WASP and Mena KO cells and when IRSp53, WAVE1, or WAVE2 were knocked down. The exclusion of Mena from the Rif pathway is plausible. The anti-capping activity of Mena is believed to facilitate filopodium formation by allowing continuous barbed end growth of microfilaments (1). By virtue of the binding of its formin homology 2 domains to the barbed end throughout filopodial microfilament extension, the actin-polymerizing mDia1 (as well as mDia2) dimer offers protection from barbed end capping proteins and thus by itself fulfills the anti-capping function (60). The actin bundling properties of *Dictyostelium* VASP (vasodilator-stimulated phosphoprotein) (61) and Eps8 (10) have been implicated in filopodium formation. A possible role for Eps8 in Rif-mediated filopodial protrusion was not investigated here, but the formin homology 2 domain of mDia2 has been reported to be capable of bundling actin *in vitro* (62), and it is possible that Rif utilizes mDia2 to fulfill this function in forming filopodia. That IRSp53 is not required for the Rif pathway raises the question of how, and through what other protein(s), Rif might bring about membrane deformation to facilitate filopodium extension. Identifying other proteins that may bind Rif directly or form protein complexes with it will help to shed light on the exact mechanism of Rif-induced filopodium protrusion.

Filopodia have been proposed to arise from lamellipodia by selective elongation and reorganization of existing lamellipodial microfilaments into bundles, based on observations in B16F1 melanoma and *Drosophila* cells. This led to the convergent elongation model for filopodium formation (63, 64). Rac acts through WAVE and the Arp2/3 complex to direct the formation of the branched microfilament networks that constitute lamellipodia and ruffles (65). If filopodial microfilaments were indeed derived from lamellipodial ones according to the convergent elongation model, suppression of the Rac pathway would negatively impact on filopodium formation. However, cells that lacked lamellipodia due to knockdown of WAVE or Arp2/3 complex were still able to put out filopodia (55). Electron microscopy studies showing that filopodial microfilaments arise from lamellipodial microfilaments (35, 63, 64) have also been challenged by the fact that intertwining of microfilaments from both structures after formin-mediated filopodium formation had occurred could give rise to the same observations, further diminishing support for the convergent elongation model (66). In this study, Rif could still form filopodia in both N-WASP WT and KO cells in the presence of RacDN. Although the ability of Rif to trigger filopodia in the presence of RacDN was not tested in N1E115 cells, many of the Rif-driven filopodia in that cell line were observed to arise independently rather than from lamellipodia. Thus, Rif filopodia form by a mechanism distinct from that described in the convergent elongation model.

Rif Interacts with mDia1 but Not mDia2 in Filopodia—mDia2 has been put forward as a Rif effector involved in filopodial protrusion (31, 51). In this study, we found that both mDia1 and mDia2 are involved in Rif-mediated filopodium formation in N1E115 cells, as evident by the decrease in number of Rif filopodia formed when either protein was knocked down. However, our AP-FRET results show that of the two, only mDia1 interacts with Rif within filopodia. Although both Rif and mDia2 were previously observed within filopodia-like protrusions in cells overexpressing both proteins, the only evidence thus far of interaction between Rif and full-length mDia2 has come from yeast two-hybrid assays (31). In immunoprecipitation experiments, Pellegrin and Mellor (31) were able to dem-

onstrate binding between Rif and a constitutively active mutant of mDia2 lacking the C-terminal Diaphanous autoregulatory domain but not full-length wild type mDia2. When we overexpressed full-length mDia2 with Rif in N1E115 cells in this study, although both proteins did appear in filopodia-like protrusions, there was no FRET between them. In contrast, the AP-FRET experiments revealed that full-length wild type mDia1 interacts with Rif within filopodia-like protrusions, providing spatial information on this interaction, which had previously only been shown to occur by immunoprecipitation assays using a constitutively active mutant of mDia1 missing the C-terminal Diaphanous autoregulatory domain and by yeast two-hybrid assays using an N-terminal fragment of mDia1 containing the GTPase binding domain (33). It is possible that mDia2 has to first be activated by another protein before the Rif-mDia2 interaction can take place, and this might explain why we did not observe FRET between Rif and full-length mDia2 in filopodia-like protrusions.

Our results indicate that mDia1 might have a more direct role than mDia2 in Rif-mediated filopodium formation. This ties in with the conclusions of Sarmiento *et al.* (50), who found that filopodium formation resulting from knockdown of both N-WASP and WAVE2 in rat mammary adenocarcinoma cells was blocked by silencing mDia1 but not mDia2. In that same study, endogenous mDia1 was detected in the filopodia of N-WASP/WAVE2 double knockdown cells and exogenous constitutively active mDia1 at the tips of the filopodia that it induced in cells not subjected to RNAi treatment (50). Although the authors ruled out Cdc42 and Rac and implicated RhoA as the trigger of the mDia1-positive filopodia that they observed, Rif was not taken into consideration and evaluated (50). In our live imaging studies, EYFP-mDia1 when overexpressed alone was sufficient to cause filopodial protrusion in N1E115 cells and was also detected within these structures, which were similar in length to those induced by Rif alone. A role for mDia1 in filopodium formation is further supported by the recent identification of a basic domain in its N terminus that localizes and anchors the protein to the plasma membrane. This would allow it to be at the tips of growing filopodia, forming actin filaments with the fast growing barbed ends pushing against the inner surface of the membrane (20).

In conclusion, we have carried out, for the first time, a quantitative analysis of Rif-induced filopodium formation and presented evidence for a novel pathway involving mDia1 that is independent of Cdc42 and Rac effectors. Ongoing work to identify Rif-interacting proteins should help to establish other components of the pathway required for filopodium formation.

Acknowledgments—We thank Harry Mellor for the generous gifts of Rif and mDia2 DNA constructs and anti-Rif antibodies, Shuh Narumiya and Sadanori Watanabe for the generous gift of anti-mDia2 antibodies and discussion, and Lim Soon Yew for help with the preparation of figures for the manuscript.

REFERENCES

1. Mattila, P. K., and Lappalainen, P. (2008) *Nat. Rev. Mol. Cell Biol.* **9,** 446–454
2. Mellor, H. (2010) *Biochim. Biophys. Acta* **1803,** 191–200
3. Machesky, L. M. (2008) *FEBS Lett.* **582,** 2102–2111
4. Dixit, R., Tiwari, V., and Shukla, D. (2008) *Neurosci. Lett.* **440,** 113–118
5. Berger, C. N., Crepin, V. F., Jepson, M. A., Arbeloa, A., and Frankel, G. (2009) *Cell Microbiol.* **11,** 309–322
6. Govind, S., Kozma, R., Monfries, C., Lim, L., and Ahmed, S. (2001) *J. Cell Biol.* **152,** 579–594
7. Krugmann, S., Jordens, I., Gevaert, K., Driessens, M., Vandekerckhove, J., and Hall, A. (2001) *Curr. Biol.* **11,** 1645–1655
8. Lim, K. B., Bu, W., Goh, W. I., Koh, E., Ong, S. H., Pawson, T., Sudhaharan, T., and Ahmed, S. (2008) *J. Biol. Chem.* **283,** 20454–20472
9. Tokuo, H., and Ikebe, M. (2004) *Biochem. Biophys. Res. Commun.* **319,** 214–220
10. Disanza, A., Mantoani, S., Hertzog, M., Gerboth, S., Frittoli, E., Steffen, A., Berhoerster, K., Kreienkamp, H. J., Milanesi, F., Di Fiore, P. P., Ciliberto, A., Stradal, T. E., and Scita, G. (2006) *Nat. Cell Biol.* **8,** 1337–1347
11. Kashiwagi, H., Shiraga, M., Kato, H., Honda, S., Sako, M., Kurata, Y., Kanakura, Y., and Tomiyama, Y. (2005) *J. Thromb. Haemost.* **3,** 361–368
12. Kim, H. J., DiBernardo, A. B., Sloane, J. A., Rasband, M. N., Solomon, D., Kosaras, B., Kwak, S. P., and Vartanian, T. K. (2006) *J. Neurosci.* **26,** 5849–5859
13. Soderling, S. H., Guire, E. S., Kaech, S., White, J., Zhang, F., Schutz, K., Langeberg, L. K., Banker, G., Raber, J., and Scott, J. D. (2007) *J. Neurosci.* **27,** 355–365
14. Ahn, S. M., Byun, K., Kim, D., Lee, K., Yoo, J. S., Kim, S. U., Jho, E. H., Simpson, R. J., and Lee, B. (2008) *PLoS ONE* **3,** e3917
15. Nakagawa, H., Miki, H., Nozumi, M., Takenawa, T., Miyamoto, S., Wehland, J., and Small, J. V. (2003) *J. Cell Sci.* **116,** 2577–2583
16. Fujiwara, T., Mammoto, A., Kim, Y., and Takai, Y. (2000) *Biochem. Biophys. Res. Commun.* **271,** 626–629
17. Faix, J., and Grosse, R. (2006) *Dev. Cell* **10,** 693–706
18. Wallar, B. J., and Alberts, A. S. (2003) *Trends Cell Biol.* **13,** 435–446
19. Young, K. G., and Copeland, J. W. (2010) *Biochim. Biophys. Acta* **1803,** 183–190
20. Ramalingam, N., Zhao, H., Breitsprecher, D., Lappalainen, P., Faix, J., and Schleicher, M. (2010) *Eur. J. Cell Biol.* **89,** 723–732
21. Watanabe, N., Kato, T., Fujita, A., Ishizaki, T., and Narumiya, S. (1999) *Nat. Cell Biol.* **1,** 136–143
22. Xie, Y., Tan, E. J., Wee, S., Manser, E., Lim, L., and Koh, C. G. (2008) *J. Cell Sci.* **121,** 514–521
23. Arakawa, Y., Bito, H., Furuyashiki, T., Tsuji, T., Takemoto-Kimura, S., Kimura, K., Nozaki, K., Hashimoto, N., and Narumiya, S. (2003) *J. Cell Biol.* **161,** 381–391
24. Yamana, N., Arakawa, Y., Nishino, T., Kurokawa, K., Tanji, M., Itoh, R. E., Monypenny, J., Ishizaki, T., Bito, H., Nozaki, K., Hashimoto, N., Matsuda, M., and Narumiya, S. (2006) *Mol. Cell Biol.* **26,** 6844–6858
25. Carramusa, L., Ballestrem, C., Zilberman, Y., and Bershadsky, A. D. (2007) *J. Cell Sci.* **120,** 3870–3882
26. Fernandez-Borja, M., Janssen, L., Verwoerd, D., Hordijk, P., and Neefjes, J. (2005) *J. Cell Sci.* **118,** 2661–2670
27. Wen, Y., Eng, C. H., Schmoranzer, J., Cabrera-Poch, N., Morris, E. J., Chen, M., Wallar, B. J., Alberts, A. S., and Gundersen, G. G. (2004) *Nat. Cell Biol.* **6,** 820–830
28. Ishizaki, T., Morishima, Y., Okamoto, M., Furuyashiki, T., Kato, T., and Narumiya, S. (2001) *Nat. Cell Biol.* **3,** 8–14
29. Goode, B. L., and Eck, M. J. (2007) *Annu. Rev. Biochem.* **76,** 593–627
30. Ellis, S., and Mellor, H. (2000) *Curr. Biol.* **10,** 1387–1390
31. Pellegrin, S., and Mellor, H. (2005) *Curr. Biol.* **15,** 129–133
32. Gad, A. K., and Aspenström, P. (2010) *Cell. Signal.* **22,** 183–189
33. Fan, L., Pellegrin, S., Scott, A., and Mellor, H. (2010) *J. Cell Sci.* **123,** 1247–1252
34. Danson, C. M., Pocha, S. M., Bloomberg, G. B., and Cory, G. O. (2007) *J. Cell Sci.* **120,** 4144–4154
35. Yang, C., Czech, L., Gerboth, S., Kojima, S., Scita, G., and Svitkina, T. (2007) *PLoS Biol.* **5,** e317
36. He, L., Wu, X., Simone, J., Hewgill, D., and Lipsky, P. E. (2005) *Nucleic Acids Res.* **33,** e61
37. Wood, W., and Martin, P. (2002) *Int. J. Biochem. Cell Biol.* **34,** 726–730
38. Peng, J., Wallar, B. J., Flanders, A., Swiatek, P. J., and Alberts, A. S. (2003)

Curr. Biol. **13,** 534–545
39. Woodring, P. J., Meisenhelder, J., Johnson, S. A., Zhou, G. L., Field, J., Shah, K., Bladt, F., Pawson, T., Niki, M., Pandolfi, P. P., Wang, J. Y., and Hunter, T. (2004) *J. Cell Biol.* **165,** 493–503
40. Miyashita, M., Ohnishi, H., Okazawa, H., Tomonaga, H., Hayashi, A., Fujimoto, T. T., Furuya, N., and Matozaki, T. (2004) *Mol. Biol. Cell* **15,** 3950–3963
41. Yang, L., Wang, L., and Zheng, Y. (2006) *Mol. Biol. Cell* **17,** 4675–4685
42. Radha, V., Rajanna, A., Mitra, A., Rangaraj, N., and Swarup, G. (2007) *Exp. Cell Res.* **313,** 2476–2492
43. Carlier, M. F., Ducruix, A., and Pantaloni, D. (1999) *Chem. Biol.* **6,** R235–R240
44. Copeland, J. W., and Treisman, R. (2002) *Mol. Biol. Cell* **13,** 4088–4099
45. Lizárraga, F., Poincloux, R., Romao, M., Montagnac, G., Le Dez, G., Bonne, I., Rigaill, G., Raposo, G., and Chavrier, P. (2009) *Cancer Res.* **69,** 2792–2800
46. Bu, W., Chou, A. M., Lim, K. B., Sudhaharan, T., and Ahmed, S. (2009) *J. Biol. Chem.* **284,** 11622–11636
47. Sudhaharan, T., Liu, P., Foo, Y. H., Bu, W., Lim, K. B., Wohland, T., and Ahmed, S. (2009) *J. Biol. Chem.* **284,** 13602–13609
48. Yang, C., Hoelzle, M., Disanza, A., Scita, G., and Svitkina, T. (2009) *PLoS ONE* **4,** e5678
49. Sigal, Y. J., Quintero, O. A., Cheney, R. E., and Morris, A. J. (2007) *J. Cell Sci.* **120,** 340–352
50. Sarmiento, C., Wang, W., Dovas, A., Yamaguchi, H., Sidani, M., El-Sibai, M., Desmarais, V., Holman, H. A., Kitchen, S., Backer, J. M., Alberts, A., and Condeelis, J. (2008) *J. Cell Biol.* **180,** 1245–1260
51. Hotulainen, P., Llano, O., Smirnov, S., Tanhuanpää, K., Faix, J., Rivera, C., and Lappalainen, P. (2009) *J. Cell Biol.* **185,** 323–339
52. McCroskery, S., Chaudhry, A., Lin, L., and Daniels, M. P. (2006) *Mol. Cell Neurosci.* **33,** 15–28
53. Loitto, V. M., Huang, C., Sigal, Y. J., and Jacobson, K. (2007) *Exp. Cell Res.* **313,** 1295–1306
54. Robles, E., Woo, S., and Gomez, T. M. (2005) *J. Neurosci.* **25,** 7669–7681
55. Steffen, A., Faix, J., Resch, G. P., Linkner, J., Wehland, J., Small, J. V., Rottner, K., and Stradal, T. E. (2006) *Mol. Biol. Cell* **17,** 2581–2591
56. Guerrier, S., Coutinho-Budd, J., Sassa, T., Gresset, A., Jordan, N. V., Chen, K., Jin, W. L., Frost, A., and Polleux, F. (2009) *Cell* **138,** 990–1004
57. Obermeier, A., Ahmed, S., Manser, E., Yen, S. C., Hall, C., and Lim, L. (1998) *EMBO J.* **17,** 4328–4339
58. Zaoui, K., Honoré, S., Isnardon, D., Braguer, D., and Badache, A. (2008) *J. Cell Biol.* **183,** 401–408
59. Eisenmann, K. M., West, R. A., Hildebrand, D., Kitchen, S. M., Peng, J., Sigler, R., Zhang, J., Siminovitch, K. A., and Alberts, A. S. (2007) *J. Biol. Chem.* **282,** 25152–25158
60. Kovar, D. R. (2006) *Curr. Opin. Cell Biol.* **18,** 11–17
61. Schirenbeck, A., Arasada, R., Bretschneider, T., Stradal, T. E., Schleicher, M., and Faix, J. (2006) *Proc. Natl. Acad. Sci. U.S.A.* **103,** 7694–7699
62. Harris, E. S., Rouiller, I., Hanein, D., and Higgs, H. N. (2006) *J. Biol. Chem.* **281,** 14383–14392
63. Svitkina, T. M., Bulanova, E. A., Chaga, O. Y., Vignjevic, D. M., Kojima, S., Vasiliev, J. M., and Borisy, G. G. (2003) *J. Cell Biol.* **160,** 409–421
64. Biyasheva, A., Svitkina, T., Kunda, P., Baum, B., and Borisy, G. (2004) *J. Cell Sci.* **117,** 837–848
65. Takenawa, T., and Suetsugu, S. (2007) *Nat. Rev. Mol. Cell Biol.* **8,** 37–48
66. Beli, P., Mascheroni, D., Xu, D., and Innocenti, M. (2008) *Nat. Cell Biol.* **10,** 849–857